Tectonophysics
September 2023, Volume 863, Pages 229989 (13p.)
https://doi.org/10.1016/j.tecto.2023.229989 https://archimer.ifremer.fr/doc/00847/95889/

Lithospheric architecture beneath the Amsterdam-St. Paul plateau, Southern Indian Ocean using the integrated gravity, magnetic and seismological study

Kumar Pankaj [1, 2, *], Singha Pabitra [2], Ghosal Dibakar [2], Jacob Jensen [3], Gupta Sandeep [1]

[1] CSIR-National Geophysical Research Institute, Hyderabad 500007, India
[2] Indian Institute of Technology Kanpur, Kanpur 208016, UP, India
[3] CSIR-National Institute of Oceanography, Dona Paula, Goa 403004, India

* Corresponding author : Pankaj Kumar, email address : pankajbhu29@gmail.com

Abstract :

Evolution of the Amsterdam-St. Paul (ASP) plateau is debated as a consequence of the Kerguelen mantle plume interaction with the South-East Indian Ridge (SEIR) or related with a weaker ASP plume origin. We performed an integrated geophysical approach using gravity and magnetic modeling along with the joint inversion of Ps receiver function and Rayleigh wave group velocity dispersion data to determine the crustal architecture, and upper mantle structure below the plateau. The gravity-magnetic model revealed that the plateau is associated with three crustal layers as basaltic layer, gabbroic layer and underplated material underlain by sedimentary strata. Our models further suggests that beneath the ASP plateau the Moho depth varies from ~6.6 to 18.0 km. Joint inversion of Ps receiver function and Rayleigh wave group velocity dispersion curve suggested the Lithosphere-Asthenosphere Boundary at depth of 50 km below the Amsterdam Island. Further seismological result suggests evidence of a Low Velocity Zone below the Moho at depth of 20–36 km which may represent a magma chamber. Our model suggests that the evolution of the ASP plateau is guided by the Amsterdam and St. Paul fracture zones, which acted as a thermal boundary confining the horizontal movement of the ASP plume. We propose that the ASP plateau is not linked with the Kerguelen plume and emphasize origin of the ASP plateau by the interaction of SEIR with the ASP plume.

Highlights

► The Amsterdam-St. Paul (ASP) plateau is associated with basaltic, gabbroic and underplated layer below sedimentary strata. ► A low velocity zones below the Moho (20–36 km depth) indicate magma chamber beneath the Amsterdam Island. ► The Lithosphere-Asthenosphere boundary is present at ~50 km depth. ► The ASP plateau might not be formed by the Kerguelen plume.

Keywords : Amsterdam-St. Paul (ASP) plateau, Integrated gravity-magnetic modeling, Joint inversion, ASP plume, Kerguelen plume, Ridge-hot spot interaction

1. Introduction

The interaction of migrating mid-ocean ridge with a near-ridge hotspot plays a significant role in the formation of oceanic plateaus such as Iceland, Azores and Galapagos (Gente et al., 2003; Johnson et al., 1972; Wilson and Hay, 1995). The ridge-hot spot interaction leads to morphological evolution of oceanic plateaus and magma production at the ridge over millions of years (Schilling et al., 1985). The magma production at the plateau depends upon the migrating plume-ridge interaction, governed by the major controlling factors (1) the plume flux and (2) the direction and rate of the spreading ridge relative to the plume (Small, 1995).

The South-East Indian Ridge (SEIR) interacted with two hot spots: the Kerguelen and Amsterdam-St. Paul (ASP) hotspots since ~40 My (Doucet et al., 2004). The Kerguelen plateau was formed when the SEIR interacted with the Kerguelen hotspot and separation of the Broken Ridge from the Kerguelen Plateau took place contemporaneously at ~40 Ma (Mutter and Cande, 1983; Tikku and Cande, 2000). Further, the ASP hot spot interacted with the SEIR and formed the ASP plateau (Fig. 1a, b) at ~10 Ma (Maia et al., 2011; Janin et al., 2012; Sibrant et al., 2019). Initially, Luyendyk and Rennick (1977) suggested that the ASP plateau was formed by the Kerguelen plume, whereas Morgan (1978) hypothesized a distinct mantle plume resulted formation of the plateau. Several geochemical studies (Ludden et al., 1980; Graham et al., 1999; Johnson et al., 2000) reported that the ASP basalt is similar to the Kerguelen plateau basalt, Broken ridge basalt and Ninteyeast ridge basalt, whereas some recent studies based on the geochemical and isotopic analysis (Doucet et al., 2004; Nicolaysen et al., 2007; Janin et al., 2012) documented evidence of distinct isotopic characteristic of the ASP basalt on

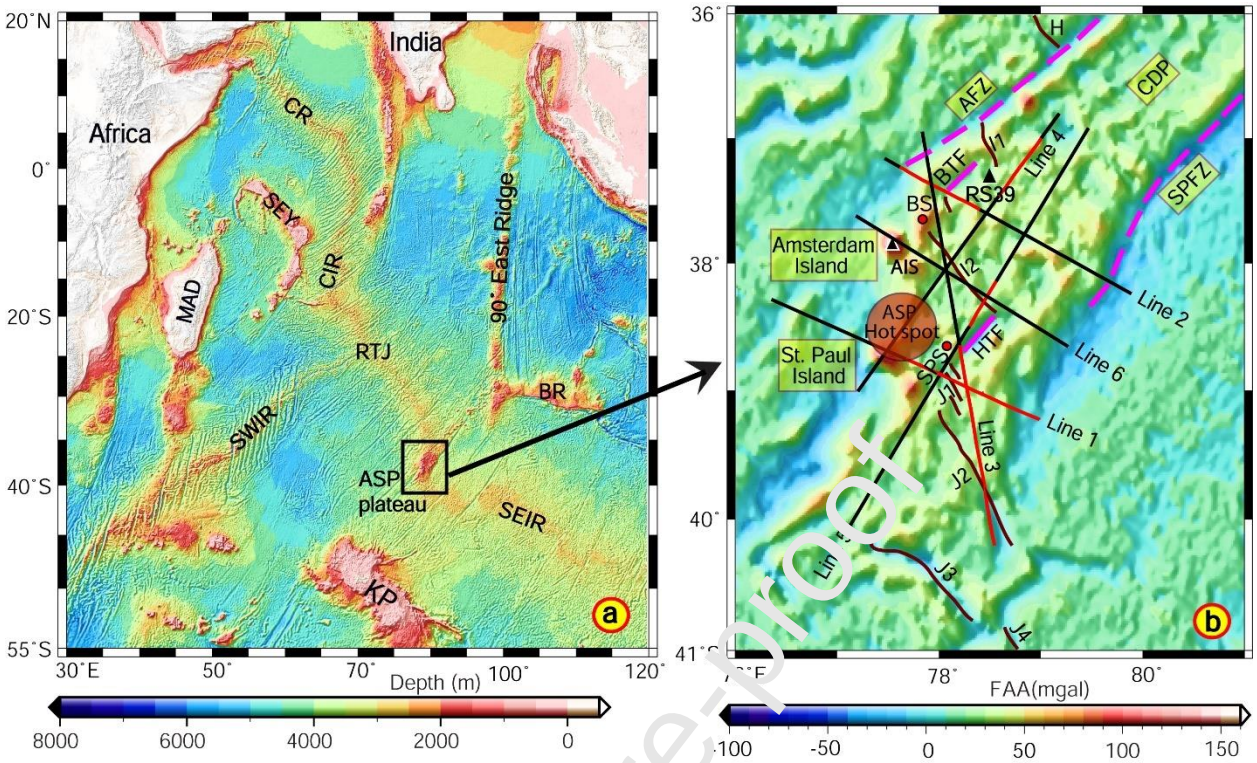

Fig.1 (a) General bathymetric map of the Indian Ocean showing major physiographic features in region. MAD: Madagascar, SEY: Seychelles, CR: Carlsberg Ridge, CIR: Central Indian Ridge, SWIR: South-West Indian Ridge, SEIR: South-east Indian Ridge, RTJ: Rodriguez Triple Junction, KP: Kerguelen Plateau, ASP: Amsterdam- St. Paul Plateau. **(b)** Detailed view of the ASP plateau over Free-air gravity anomaly map. Map showing selected transects (Line 1, Line 2, Line 3, Line 4, Line 5, and Line 6) along which integrated gravity-magnetic modeling was carried out. Satellite bathymetry and gravity data is available along thick black solid segment of transects whereas satellite bathymetry and gravity along with ship-borne magnetic data is available along thick red solid segment of transects. Black triangle represents refraction station named RS-39 (taken from Francis and Raitt 1967) and another black triangle represents AIS station which is a permanent broadband station located on the Amsterdam Island. Solid red circle represents seamounts lie on the ASP plateau. Red color semi-transparent circle represents probable location of the ASP hotspot (Maia et al. 2011). *H*, *I1*, *I2*, *J1*, *J2*, *J3* and *J4* represent ridge segments of the SEIR (Taken from Conder et al., 2000). BS: Boomerang Seamount, CDP: Chain of Dead Poet, AFZ: Amsterdam Fracture Zone,

SPFZ: St. Paul Fracture Zone, BTF: Boomerang Transform Fault, HTF: Hillegom Transform Fault, SPS: St. Pierre Seamount.

different locations on the plateau. Presently, two school of thoughts exist on the formation of the ASP plateau. A group of studies (Graham et al. 1999; Doucet et al., 2004; Nicolaysen et al., 2007) supported a secondary hotspot known as the ASP hotspot was responsible for the formation of the ASP plateau within a time span of ~10 My (Janin et al., 2011; Maia et al., 2011; Janin et al., 2012; Sibrant et al., 2019), whereas, few studies (Luyendyk and Rennick, 1977; Bredow and Steinberger, 2018) reported the plateau origin to be associated with the Kerguelen plume.

Several geophysical studies like bathymetry, gravity, and magnetic (e.g., Royer and Schlich, 1988; Scheirer et al., 1998; Scheirer et al., 2000; Conder et al., 2000; Janin et al., 2011; Maia et al., 2011) have been conducted over the ASP plateau to date. The marine magnetic studies suggested several SEIR ridge segments running over the ASP plateau (Royer and Schlich, 1988; Conder et al., 2000). Gravity studies suggested ~13 km thick crust over the plateau (Scheirer et al., 2000; Maia et al., 2011), while Dubinin et al. (2017) suggested 12-16 km thick crust over the plateau. However, these studies could not comment on the origin of the mantle plume that caused formation of the ASP plateau convincingly.

Global tomographic studies (Zhao, 2007) indicate low *P*-wave velocity originating from the core-mantle boundary in the entire mantle beneath the region southwest of the Amsterdam Island which suggest that plume may be originating from the core-mantle boundary. However, the study was not indicative to the fact whether the low *P*-wave velocity associated with the plume had any link up with the ASP plateau or not. Another study, using S-receiver function technique (Kumar et al., 2007) reported the depth of the Moho at ~14 km and the Lithosphere-Asthenosphere Boundary (LAB) at a depth of ~49 km beneath the Amsterdam Island. However, a detailed seismological study at the Amsterdam Island and of the ASP plateau is not available to date.

Present study thus aims to understand the crustal architecture and upper mantle structure beneath the ASP plateau integrating bathymetry, gravity, magnetic and seismological datasets. The primary objectives are (i) to determine the crustal

architecture of the ASP plateau, (ii) to investigate the upper mantle structure below the Amsterdam Island, (iii) to find any linkage between the ASP plateau and the Kerguelen plume. (iv) to analyze the ASP hotspot-SEIR interaction and present tectonic configuration of the ASP plateau.

2. Regional tectonic setting

The ASP plateau (Fig. 1) is a complex structure that formed by ridge-hot spot interaction (Janin et al., 2011; Maia et al., 2011). The plateau lies in the southern Indian Ocean over the SEIR with intermediate spreading (Conder et al., 2000) and the ridge separates the Australian plate in NE from the Antarctic plate in SW. The ASP plateau can be delimited by the depth ranges from 2300-2800 m, having an area of >30000 km^2 (Scheirer et al., 2000). The plateau is bounded by the Amsterdam Fracture Zone (AFZ) to the north and the St. Paul Fracture Zone (SPFZ) to the south (Royer and Schlich, 1988; Janin et al., 2011; Maia et al., 2011). The Chain of Dead Poets (CDP), located to the NE of the ASP plateau (Johnson et al., 2000; Janin et al., 2011) is a chain of submarine volcanoes (Fig. 1a) which was formed since ~20 Ma and suggested to be a trace of the ASP hotspot (Janin et al., 2011; Janin et al., 2012). The ASP plateau is mostly submarine except two subaerial features, the Amsterdam and St. Paul islands which are located ~100 km apart from each other and are recently formed (~0.4 Ma) (Watkins et al., 1975). These two islands are structurally separated by a SW-NE transform fault (Fig. 1b)

The plateau hosts an active seamount, the Boomerang seamount (Johnson et al., 2000; Nicolaysen et al., 2007), which is an active submarine volcano located ~18 km NE of the Amsterdam Island (Johnson et al., 2000). Another prominent seamount, the St. Pierre seamount lies east of the St. Paul Island (Nicolaysen et al., 2007) (Fig. 1b). A set of four SEIR ridge segments *I1*, *I2*, *J1* and *J2* were identified by Royer and Schlich (1988), which later modified as six ridge segments *I1*, *I2*, *J1*, *J2*, *J3* and *J4* (Fig. 1b) by Conder et al. (2000). They further suggested that the ridge segments over the plateau shows *en echelon* segmentation and oblique spreading and the southward propagation of the segment *J2*. They further suggested that the segment *I* include two primary spreading centers *I1* and *I2* with an additional short and active spreading center

between the two, which is grouped with *I2* segment. Scheirer et al. (2000) reported that segments *I1* and *I2* are separated by a recently formed discontinuity known as the Boomerang Transform Fault (BTF) (Fig. 1b). Segment *I2* is comprised of northern shorter section (20 km) and a southern longer section (100 km) which is limited in the south by the Hillegom Transform Fault (HTF). Further southward, extending from the HTF, segment *J1* comprises of three short (<50 km), sigmoidal, *en echelon* segments which are oblique to spreading direction. Segment *J2* is a propagating rift crossing the southern edge of the plateau, whereas segments *J3* and *J4* (separated by ~15 km) are off the ASP plateau (Conder et al., 2000) (Fig. 1b).

3. Datasets

3.1 Bathymetry and Potential field data

In this study, we used ship-borne bathymetry, gravity and magnetic data along with satellite bathymetry and gravity data (Fig. 1b). Ship-borne bathymetry data is obtained with a special request to Ifremer Marine Geosciences, LOUBRIEU Benoît, ROYER Jean-Yves, MAIA Marcia (Bathymetry - Saint-Paul and Amsterdam - synthesis, 2020). Ship-borne gravity and magnetic data are received with a special request to Hydroamsterdam oceanographic cruise (BEUZART Paul, 1984) and the data were sampled at 1 minute. The Free-Air Gravity Anomalies (FAA) are obtained after editing/deleting the spikes/erroneous data points from the data file. Magnetic data are corrected by removing spikes and the total magnetic field intensity data are reduced to residual magnetic anomalies by subtracting the International Geomagnetic Reference Field (IGRF) of appropriate epoch. We then used the satellite altimetry derived bathymetry and FAA data as the obtained ship-borne data collected in 1984 and is sparse along the track line. We, therefore, used the corresponding satellite bathymetry and gravity data along the track line for the present study as the ship-borne and satellite data are of good correlation. We extracted the satellite derived bathymetry data from 'Bedrock' version of ETOPO1 global relief grid data (Amante & Eakins, 2009) (https://www.ngdc.noaa.gov/mgg/global). We extracted the FAA data from global marine gravity data 'grav.img.24.1' (Sandwell et al., 2014) (https://topex.ucsd.edu/pub/global_grav_1min).

3.2 Seismic refraction and palaeomagnetic data

We have also used the public domain seismic refraction and palaeomagnetic results of the study area. We have compiled the results of seismic refraction data from station RS-39 (Fig. 1b, Francis and Raitt, 1967) to derive the crustal layer density over the plateau as gravity constraint for integrated gravity-magnetic modeling. Palaeomagnetic properties of lava flow found on the ASP plateau are very much limited. Waltkins et. al. (1975) and Carvallo et al. (2003) have collected samples for palaeomagnetic study over the St. Paul and the Amsterdam islands, respectively. Palaeomagnetic studies provided the magnetic properties of lava flow over these two islands and the results are used here as magnetic constraint for integrated gravity-magnetic modeling.

3.3 Seismological data

We used three component seismograms from the permanent broadband station - AIS (Amsterdam Island, Fig. 1b) available from IRIS (Incorporated Research Institutions for Seismology) data centre (https://ds.iris.edu/wilber3/find event). We have considered three high magnitude teleseismic earthquake events, lying in the epicentral distance ranging from ~ 4940 to 4974 km, with magnitude Mw >7.2. These earthquakes occurred at the Sunda subduction zone (Table 1). We have selected these earthquakes since these events are located close to each other and thus the seismic waves sample similar region.

Table 1: Earthquake event catalogue used for joint Inversion of receiver function and dispersion curve.

Date	Origin Time (Hr:min:sec)	Latitude (^oN)	Longitude (^oE)	Depth (km)	Back Azimuth (^oN)	Epicentral Distance (km)	Magnitude (MW)
2004	00:58:52	3.4125	95.9012	26.1	26.6678	4939.6	9.0

-12-26					4		
2008-02-20	08:08:31	2.7634	95.9644	31.4	27.08476	4871.46	7.3
2010-05-09	05:59:42	3.7328	96.0278	42.3	26.67456	4973.93	7.3

Also, the high magnitudes were beneficial for phase identification of receiver function and dispersion curve analysis which are used for this study and preclude the use of any additional frequency filters for noise elimination. We used 90 minutes of time length of these seismograms to include both the body and surface waves.

4. Methodology

4.1 Integrated potential field forward modeling

To find out the crustal architecture of the ASP plateau, we derived several crustal models using 2D integrated gravity-magnetic forward modeling approach across the plateau. The computational scheme is based on the method of Talwani et al. (1959) and algorithms of Won and Bevis (1987). Crustal models were generated by GM-SYS module of the Oasis Montaj software using the two-dimensional modeling method of Talwani and Heirtzler (1964) with the help of gravity and magnetic data under available geological and geophysical constraints. The objective for integrated gravity-magnetic modeling in this study is to obtain a plausible crustal structure, which is compatible with the observed anomalies and known constraints.

We carry out the integrated gravity-magnetic modeling along several transects (Line 1, Line 2, Line 3, Line 4, Line 5 and Line 6; Fig. 1b), which traverse in NW-SE (Line 1, 2 and 6), SW-NE (Line 4 and 5) and NNW-SSE (Line 3) directions across the ASP plateau crossing both the St. Paul and Amsterdam Islands (Fig. 1b). We chose Line 6 in such a way that it crosses the Amsterdam Island. Due to unavailability of magnetic data over the island, we only perform the gravity modeling along the transect. Since there is limited magnetic data available on the ASP plateau along these transects, they are

extended in either direction or both directions to cover the whole plateau area. We prepared the initial models along transect using sediment thickness (Straume et al., 2019) and published seismic refraction (Francis and Raitt, 1967) results. For that, we derived the densities of different crustal layers below the ASP plateau from refraction seismic velocity data from station RS-39 (Francis and Raitt, 1967) using Brocher formula (Brocher, 2005). For the entire profile, we considered the densities of water, sediments, crustal layers - 2, 3, 4 and upper mantle as 1.03, 1.97, 2.61, 2.89, 3.15 and 3.3 g/cm^3, respectively. The results of paleomagnetic study over the ASP plateau (Waltkins et. al., 1975; Carvallo et al., 2003) provided magnetic constraints and the magnetic parameters, which are used for the integrated modelling, are presented in Table 2. Crustal architecture of the ASP plateau is derived from the database prepared from geological models and is discussed in section 5.

Table 2: Magnetic parameters used for modeling of magnetic anomaly in the present study.

Geological body	Magnetic Polarity	Magnetic Parameters (SI)			
		Susceptibility	NRM (A/m)	Inclination (°)	Declination (°)
Basaltic flow	Normal	0.001813	8.49	-57	356.3
Intrusive	Normal	0.001813	8.49	-57	356.3
	Reverse	0.001813	8.49	57	356.3

4.2 Mantle Bouguer Anomaly (MBA) and Vertical Gravity Gradient (VGG) calculation:

The FAA data contains the combined gravity effects from seafloor topography, sediments, crust, and mantle density anomalies (Georgen et al., 2001). Mantle Bouguer Anomaly (MBA) of the study area is computed by subtracting the gravity effects of the topography and of crust-mantle interface (assuming a normal crustal thickness of 6 km) from the FAA. Gravity effects of these interfaces are computed using Fast Fourier Transform (FFT) algorithm (Parker, 1972). Densities of water, crust, and mantle were used as 1.03×10^3, 2.7×10^3, and 3.3×10^3 kg/m^3, respectively. Besides MBA, we also

estimate the Vertical Gravity Gradient (VGG) which is the second derivative of the earth's gravity field. VGG is used in the present study to depict the edges of shallow features such as plateau, volcanoes and seamounts based on lateral density variation.

4.3 Seismological data analysis

To complement integrated gravity-magnetic modelling described in section 4.1 and 4.2 using a better constrain S-wave velocity-depth model, we carry out the joint inversion of the Receiver Function (RF) and dispersion datasets (Ammon et al., 1990; Julia et al., 2000; Özalaybey et al., 1997; Gupta et al., 2016).

4.3.1 RF data preparation

The processing and analysis of the data are performed using the Computer Program in Seismology (CPS) (Herrmann, 2013). An initial preprocessing of the data such as demean, detrend and instrument correction are applied before further analysis. For RF preparation, we pick the onset of the *P* waves and window the data between 10-50 seconds before and after the P arrival. The traces are then rotated to radial and transverse components. An iterative time domain deconvolution (Ligorria and Ammon, 1991) is performed between the radial and the vertical components to isolate the Ps phases. We use lower Gaussian factor here as our objective is to study the lithospheric structure. We use a Gaussian filter width (Gw) of 1.6, which corresponds to a low pass filter with a corner frequency of ~0.8 Hz (Ligorria and Ammon, 1991). We chose a Gaussian factor of 1.6 to filter the low frequency impulses.

4.3.2 Dispersion data preparation

We window the Rayleigh wave segments from the vertical component to compute the dispersion curves. The dispersion curves of group velocity for fundamental mode are computed in the period range of 2-100 seconds using Multiple Filter Analysis (MFT) technique (Bhattacharya, 1983; Herrmann, 1973) to sufficiently retrieve the information of the crust and upper Mantle.

4.3.3 Joint Inversion

We then use the preconditioned RF and dispersion datasets to perform the joint inversion using the program 'joint96' (Herrmann, 2013), which is a linearized inversion scheme based on damped least squares technique (Menke, 1984). The two important parameters which are used to produce a reliable estimate of the S wave velocity structure and stabilize the inversion are (i) damping factor and (ii) influence parameter. The damping factor which controls the model stability and resolution are fixed at 0.5. The influence parameter which is a linear combination of prediction errors from the receiver function and dispersion terms provides weightage to individual datasets for inversion, is also fixed as 0.5 (Julia et al., 2000). We chose to give equal weightage to both the datasets. Since a priori information from high resolution seismic data is not available on the Amsterdam Island. Therefore, we chose a constant starting model with S-wave velocity of 4.5 km/s and assuming Moho down to depth of 100 km. We also employ layer smoothening and weightage. We smoothen the upper 20 km and apply the maximum layer weightage starting from the first layer down to a depth of 50 km and a gradual decrease in weightage up to a depth of ~85 km and greater. We iterate the inversion process for 30 times for fixed layer thickness and variable velocity and density. A flow chart of the processing step is depicted in Figure 2.

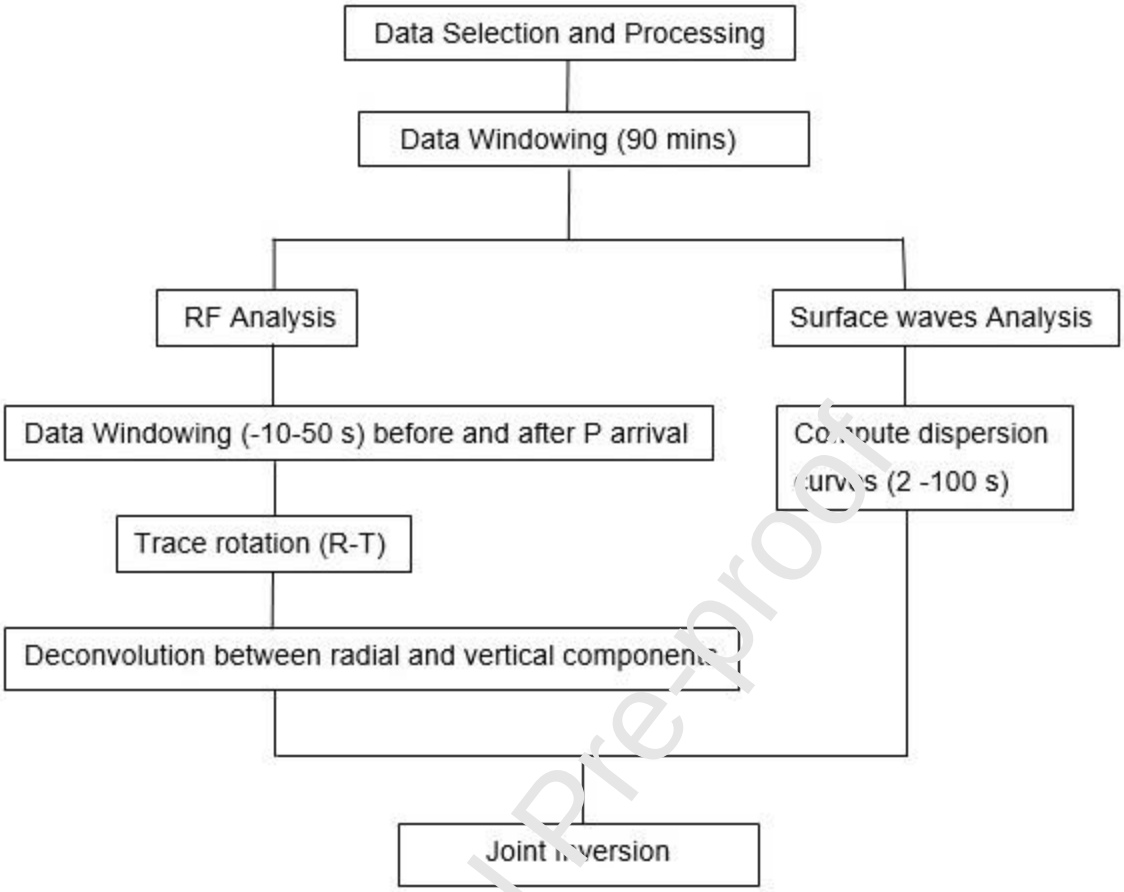

Fig. 2 Complete flow chart for the joint inversion of Receiver function and dispersion curve

5. Results and Interpretation

5.1 Crustal architecture of the ASP plateau

Crustal architecture of the ASP plateau is derived from the geological models (Fig. 3 and supplementary material S1) which are generated using integrated gravity-magnetic modeling along selected transects. FAA ranges from -12 to 153 mGal over the plateau where maximum anomaly is observed along the Amsterdam Island and minimum anomaly along the western side of the plateau (Fig. 3 and supplementary material S1), whereas the magnetic anomaly ranges from -900 to 1500 nT. The results reveal three crustal layers: 2, 3 and 4 below the sedimentary layer. Based on the refraction velocity

data from station RS-39 (Fig. 1b, Fransis and Raitt, 1967), we suggest crustal layer 2 (Vp = 4.52 km/s), 3 (Vp = 6.73 km/s) and 4 (Vp = 7.61 km/s) overlie the Moho (Vp=8.3 km/s). Moho density (~3.3 g/cm^3) is derived using Brocher formula (Brocher, 2005) from Vp data of an adjacent refraction station RS-38 (Fransis and Raitt, 1967). Christeson et al. (2019) suggested that oceanic crustal layer 2 show a velocity of Vp=4.6 km/s for 10.5 Ma, which is similar to crustal layer 2 (Vp=4.52 km/s) of the ASP plateau formed since ~10 Ma (Maia et al. 2011). Condie (2016) suggested that below the oceanic plateau, the velocity of lower crust varies almost uniformly (6.7 to 6.9 km/s) and an underplated layer shows the velocity ranging from Vp ~ 7.2-7.7 km/s. The Vp for a magmatic underplated crust is estimated within a range of 7.5-8.0 km/s (Watts et al., 1985; Caress et al., 1995; Charvis et al., 1999). Considering interpretation from this study and previous results, we classify crustal layer 2, 3 and 4 as layer 2 of oceanic crust or basaltic lava flow (Vp = 4.52 km/s), layer 3 of oceanic crust (Vp = 6.73 km/s) and underplated crust (Vp = 7.61 km/s). Previous studies over oceanic plateaus like Iceland (Darbyshire et al., 2000), Azores (Spieker et al., 2018) and Galapagos (Sallarès et al., 2005) also suggested similar type of crustal layering. The results on all the crustal layers are described in detail in following section.

5.1.1 Sedimentary layer

The integrated gravity-magnetic modeling results suggest that the thickness of the sedimentary layer varies from few meters to ~ 2.1 km over the ASP plateau and seems to increase beyond the boundary of the plateau. Minimum sediment thickness is present over the Amsterdam and St. Paul islands whereas maximum sediment thickness is observed at the western boundary of the plateau coinciding with the AFZ (supplementary material S1.1-S1a-Line 2).

5.1.2 Crustal layer 2 (Basaltic layer)

Crustal layer 2 is interpreted to be a basaltic layer with thickness varying from 1.1 to 5.5 km over the plateau. The minimum basaltic thickness is observed along the eastern end of the ASP plateau near the SPFZ (Fig. 3a, c and supplementary material S1). The maximum thickness of basaltic layer is interpreted at adjacent eastern side of the St.

Paul Island (Fig. 3a). Basaltic thickness at the western end of the plateau is also very less and controlled by the AFZ.

5.1.3 Crustal layer 3 (Gabbroic layer)

The model suggests that the crustal layer 3 or lower oceanic crust (Gabbroic layer) shows a thickness ranging from 2.2 to 9.5 km over the plateau. The minimum thickness of ~2.2 km is interpreted at the western end of the plateau whereas maximum thickness of the layer 3 is interpreted at adjacent eastern end of the St. Paul Island (Fig. supplementary material S1.3-S1c-Line 4).

5.1.4 Crustal layer 4 (underplated crust)

The results suggest that the layer 4 represents underplated crust with a maximum thickness of ~2.1 km (supplementary material S1.3-S1a-Line 2) below the St. Paul Island. We do not observe the underplated layer present below the ridge segments and volcanic centers. Scheirer et al. (2000) also reported evidence of significant underplated materials below the ASP plateau. Present study shows that underplated material is only present under the ASP plateau and absent beyond the ASP boundary.

5.1.5 Moho

The maximum Moho depth of ~18 km is observed below the St. Paul Island (Fig. 3a and supplementary material S1.3-S1c-Line 4) and ~16.5 km below the Amsterdam Island (Fig. 3c). The Moho depth decreases up to 6.6 km at the eastern part of the plateau which is associated with the AFZ. Further at the western part, the Moho is interpreted to be shallow

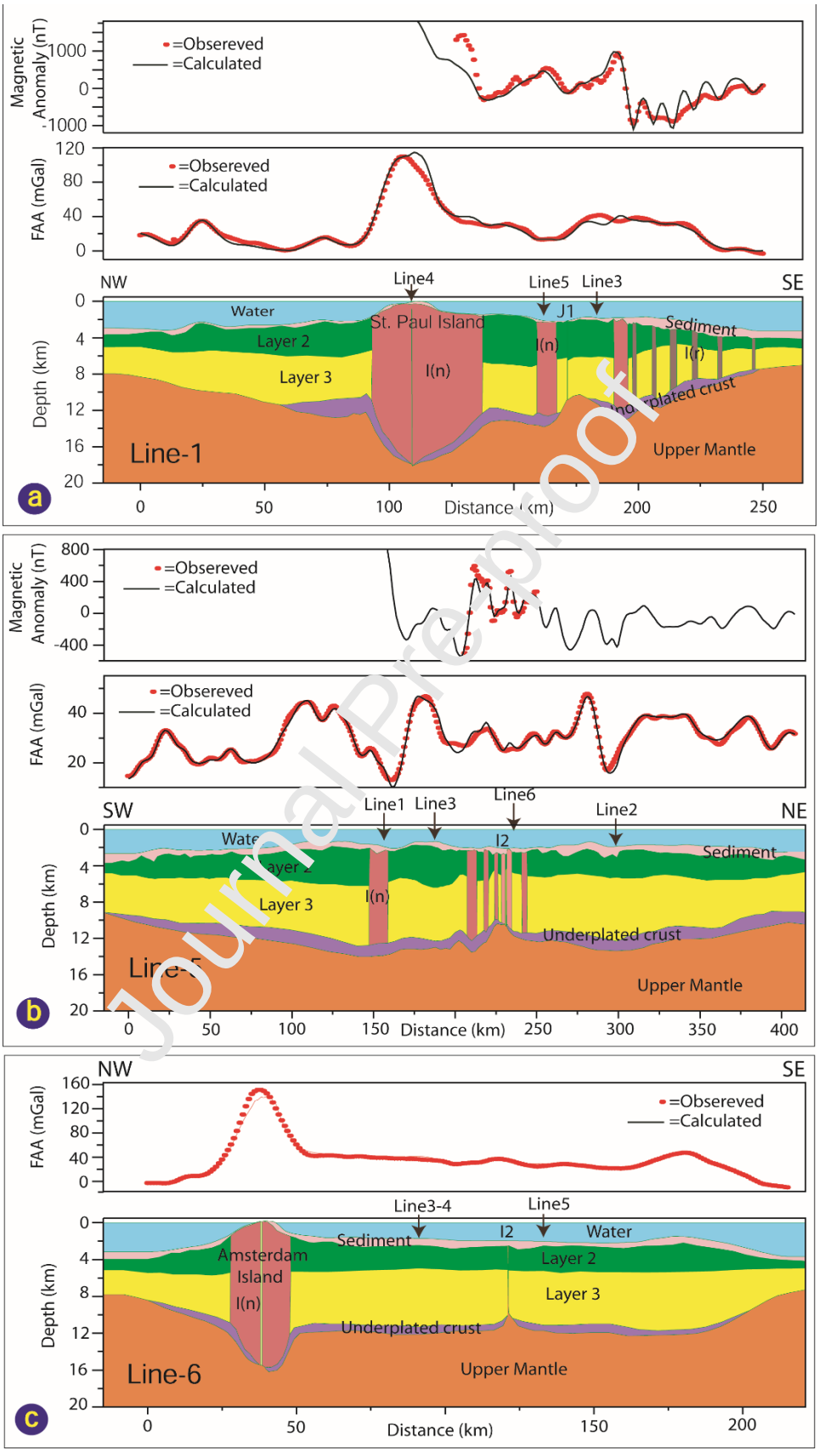

Fig. 3a Crustal model derived along Line 1. Density for magmatic intrusive body is 2.80 g/cm^3. Magnetic parameters used in anomalies computation are mentioned in Table 2. I (n): Magmatic intrusive body with normal polarity, I (r): Magmatic intrusive body with reverse polarity, FAA: Free-air anomaly. **3b** Crustal model derived along Line 5. **3c** Crustal model derived along Line 6.

at a depth of 7.5 km and is associated with the SPFZ. Our results suggest a deeper Moho below the ASP plateau and shallower beyond the plateau. The Moho depth is observed to be ~10.2 km northeast of the ASP plateau towards the CDP volcanic chain and the crust below it is associated with a ~1 km thick underplated material (Fig. 3b and supplementary material S1.3-S1c-Line 4).

5.1.6 Crustal thickness

The difference of average cumulative thickness of water plus sediment (~2.5 km) from the Moho depth represents the average crustal thickness of the ASP plateau. However, only a thin veneer of sediment is observed on both the islands with less water column thickness which is negligible relative to the crustal thickness and to reduce from the Moho depth. Hence, we get the crustal thickness ranging from ~6.6 to 18 km over the ASP plateau (Fig. 3 and supplementary material S1), where the maximum thickness of ~18 km is observed below the St. Paul Island. The earlier studies by Scheirer et al. (2000), Conder et al. (2002) and Maia et al. (2011) suggested a maximum crustal thickness of ~12 km below the St. Paul Island. However, Dubinin et al. (2017) suggested that crustal thickness near the St. Paul and Amsterdam islands could reach up to 12-16 km; our results are in good agreement with these studies. The present study suggests absence of lower oceanic crust and very thin layer of underplated crust below the St. Paul and Amsterdam islands, displaying a crustal thickness of ~18 and ~16.5 km, respectively.

5.1.7 Magmatic activity

There are several magmatic intrusive bodies (width of 2-11.5 km) of normal and reverse polarity interpreted in the crust of the ASP plateau (Fig. 3 and supplementary material

S1) and those might have played an important role in increasing the thickness of basaltic layer. Quilty (2007) reported presence of Rhyolitic dikes in crust of the St. Paul Island on the ASP plateau.

5.2 Results of jointly inverted receiver function and dispersion data for the ASP plateau

The velocity variation of different crustal layers is not much differentiated. It can be attributed to the limited resolution associated with the long wavelengths of teleseismic events. The longer wavelengths and low frequencies could detect large-scale features such as the Moho, LVZ, and LAB. Furthermore, the theoretical estimation of vertical resolution of receiver function relies on approximating the dominant wavelength. Empirical relationship suggests that the depth of resolution of the inverted RF's is equal to half of the converted (Ps) wavelength (Bostock and Rondenay,1999 and Rychert et al., 2007). Therefore, considering an average Vs of 3.8 km/s and frequency of 0.8 (Gaussian width 1.6) Hz the minimum resolvable depth would be ~ 4.75 km. Therefore, the minimum layer resolution is 2.5 km.

Joint inversion of both the datasets shows promising results. We can observe that the RF's and the dispersion curve both shows that the predicted results are well correlated with the observed data (Fig 4a, b). The *S*-wave velocity in the crust ranges from 3-4 km/s. (Fig. 4c). These velocities resemble with layer 2 and 3 of normal oceanic crust. However, the thickness of the crust is greater than two times as compared to normal oceanic crust (~7 km) (White et al., 1992).

At a depth of 12 -16 km the velocity varies from ~ 3.9-4.2 km/s. This range of the velocities represents intermediate velocities between the lower oceanic crust and Moho (White et al., 1992). Brink and Brocher (1987) reported that transitional velocities at crust-mantle boundary indicates an anomalous plutonic complex at Oahu ridge, Hawaii. Similar, transitional velocities are observed along the hotspot track of LA Réunion which is attributed to the magmatic underplating (Gallart et al., 1999). Evidence of magmatic underplating has also been reported at different volcanic hotspot islands (Caress et al., 1995; Grevemeyer et al., 2001; Contreras-Reyes et al., 2010; Gupta et al., 2010).

Therefore, the transitional velocity from this study likely represents an underplated crust which may be a result of the magmatic activity.

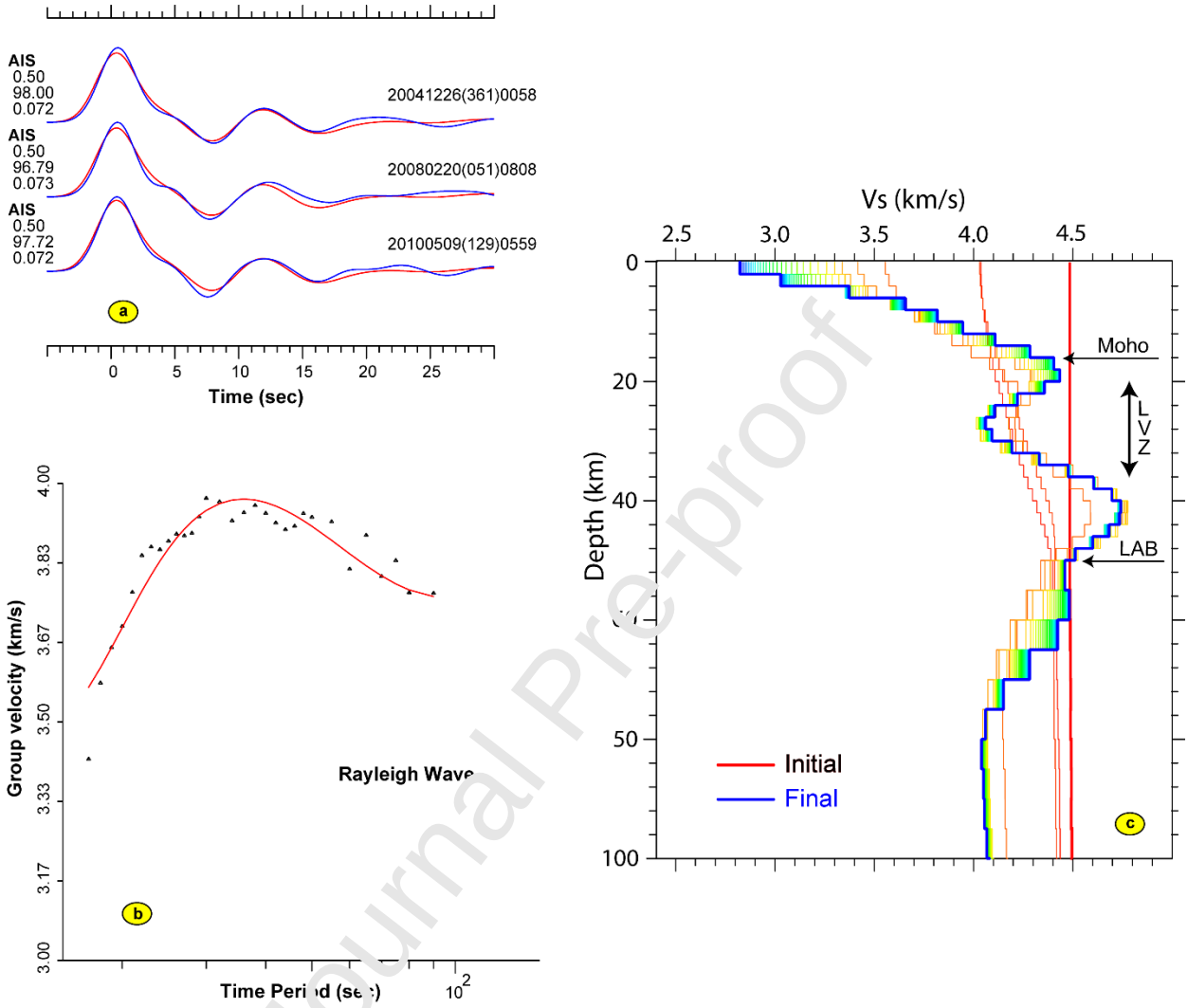

Fig. 4a Observed (red) and predicted (blue) Radial Receiver Functions. **4b** Observed (black dots) and modelled (continuous red line) dispersion curves in the period range of 2-100 seconds. **4c** Final velocity model (continuous blue line) obtained after Joint inversion of RF's and dispersion curve. The continuous red line at Vs=4.5 km is the initial velocity model.

We identify the Moho at a depth of 16 km corresponding to Vs 4.3 km/s which is also in good agreement with the integrated gravity-magnetic modeling (~16.5 km) described in section 5.1.5 and the results (14 km) from earlier studies (Kumar et al., 2007). Further, we also observe a significant low velocity zone (~ 4.0 Km/s) at a depth of ~20-36 km

(Fig. 4c) which may be a result of magma ponding/chamber and it is located immediately below the Moho. Another LVZ of ~ 4.4 km/s is observed at a depth of ~ 50 km (Fig. 4c) and seems to be associated with the Lithosphere-Asthenosphere Boundary (LAB). Analyzing Sp receiver functions, Kumar et al. (2007) reported the LAB at the depth of 49 km which is in good agreement with the result of this study.

5.3 Results on the VGG and MBA analysis

The VGG map (Fig. 5a) clearly shows the maximum horizontal density variation along several shallow features mainly fracture zones, seamounts, islands and ridge segments. The Amsterdam Island, St. Paul Island, Boomerang seamount and St. Pierre seamount are clearly visible on the VGG map as it shows high gravity gradient whereas BTF and HTF are associated with negative gravity gradient anomaly. A large variation of VGG is observed along the AFZ and SPFZ which are located north and south of the plateau, respectively. Southern part of the SPFZ is not clearly identifiable close to the ridge segments *J1*, *J2* and *J3* in the VGG map and therefore, difficult to mark its boundary at this region. The VGG map clearly shows that the ASP plateau is morphologically limited between these two fracture zones.

Mantle Bouguer Anomaly (MBA) value arises due to changes in density of crustal and mantle structure. Negative MBA value indicates mass deficiency arising either from a thicker crust or low-density material or both whereas positive MBA indicates excess mass which arises either from a thinner crust or high-density material or both. The MBA map (Fig. 5b) indicate that the ASP plateau is associated with relatively negative MBA compared to the surrounding oceanic crust. Further, MBA value decreases below the region between the Amsterdam and St. Paul islands. The SEIR segments outside the plateau *H*, *J3*, *J4* and fracture zones are also reflected in the MBA map whereas ridge segments *I1*, *I2*, and *J1* are not visible. Further, the ridge segment *J2* is partly visible in its southern part and not identifiable in its northern part in the map. The MBA map clearly indicates that the ASP plateau is associated with negative MBA and limited between the AFZ and SPFZ. Outside these two fracture zones, MBA drastically increases and clearly demarcate the ASP plateau boundary.

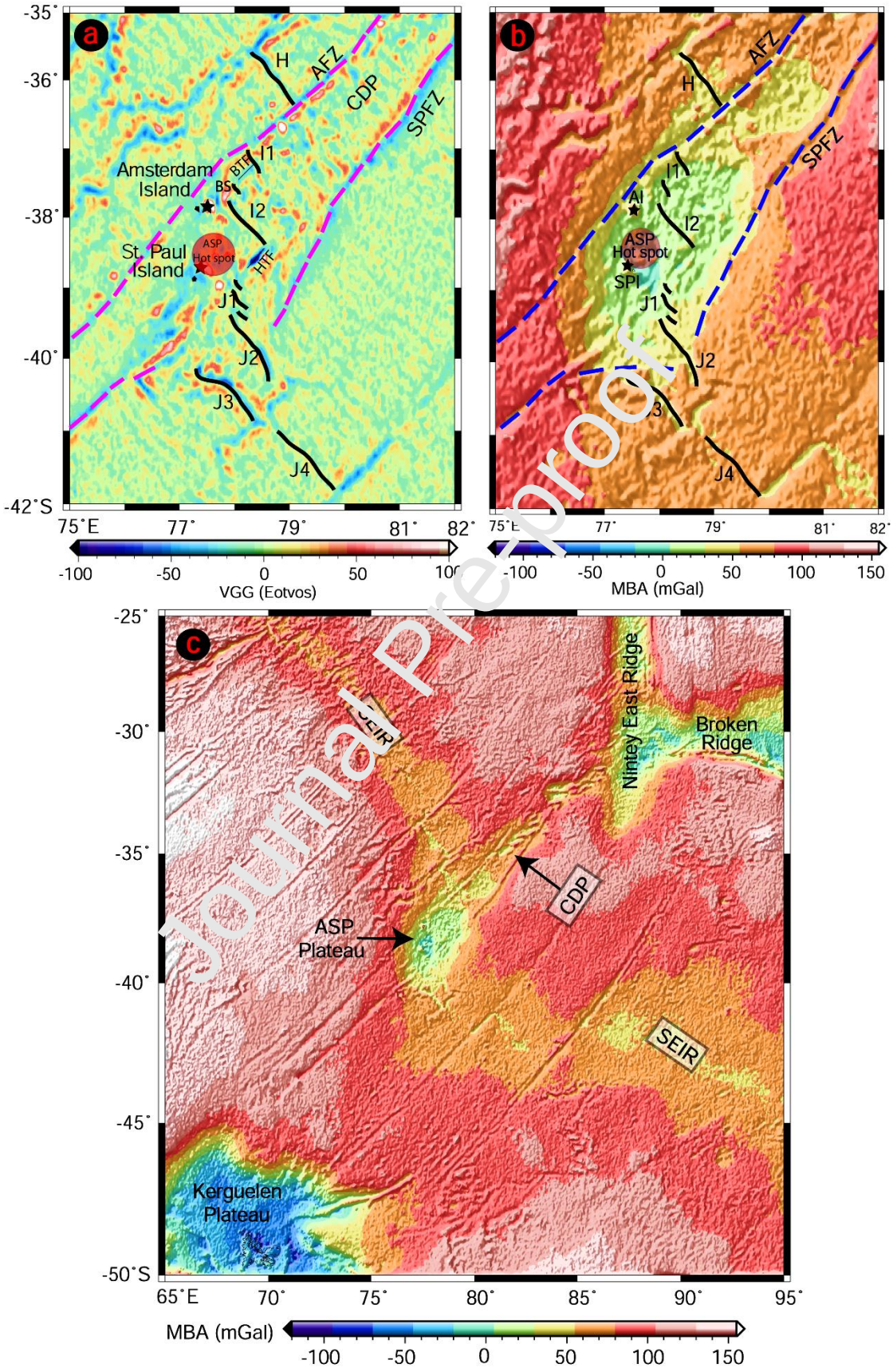

Fig. 5a Vertical Gravity Gradient (VGG) map of the study area. Black solid stars represent Amsterdam and St. Paul Islands. **5b** Mantle Bouguer Anomaly (MBA) map of the ASP plateau. AI: Amsterdam Island, SPI: St. Paul Island. Other details are given Fig. 5a. **5c** Mantle Bouguer Anomaly map of the Indian Ocean. Other details are given Fig. 5a.

6. Discussion

6.1 Discussion on the Crustal architecture of the ASP plateau

Integrated gravity-magnetic modeling results suggest that there is three crustal layers interpreted below the sedimentary layer: basaltic layer, gabbroic layer and underplated layer associated with the ASP plateau.

Evidence of maximum sediment thickness at the northwest part of the ASP plateau along with the AFZ clearly indicate that the AFZ has played a major role in controlling the sediment deposition at the fracture zone. Similarly, average sediment thickness of ~ 1 km at the southeastern part of the ASP plateau along the SPFZ, also indicates the role of SPFZ in the sediment deposition. Further, very thin basaltic layer along the eastern and western boundary of the ASP plateau near the SPFZ and AFZ respectively, suggest influence of both the fracture zones in controlling the basaltic thickness (Fig. 3 and Supplementary material S1). Maia et al. (2011) suggested that SPFZ was unstable at ~0.9 Ma when the crustal thickness started decreasing and a less magmatic accretion regime resulted at the transform discontinuity. Maximum basalt thickness adjacent to the St. Paul Island (Fig. 3a) further suggests a magma rich regime at these locations. Previous studies (Janin et al., 2011; Maia et al., 2011) suggested present location of the ASP hot spot below the crust between St. Paul and Amsterdam islands and might be the reason for the maximum basaltic thickness. The results further suggest absence of underplated material below ridge segments and volcanic centers which may be due to the continuous magma supply beneath these zones. Graham et al. (1999) suggested that the plume has been feeding the ridge segments *I1*, *I2* and *J1* on the ASP plateau and might led to the absence of underplating. Present study shows underplated material below the ASP plateau but absent beyond the fracture zones, which indicates that the plume is not affecting the crust outside the fracture zones which

mark the boundary of the ASP plateau. Francis and Raitt (1967) have shown absence of a layer having velocity range of 7.1-7.6 km/s (underplated layer) at the refraction station RS-38 located outside the ASP plateau, which support our result that the adjacent oceanic crust is not affected by the plume. Other studies (Royer and Schlich, 1988 and Dubinin et al., 2017) suggested that AFZ and SPFZ (Fig. 5a, b) behaved as a thermal barrier of the ASP hot spot activity limiting the magmatic underplating between these fracture zones. Present study suggests crustal thickness in the range of ~6.6 to ~18 km within the ASP plateau caused by variation in basaltic thickness as well as accretion of underplated material below the ASP plateau. The crustal thickness variation within the plateau indicates a variable melt supply (Janin et al., 2011) caused by high and low magmatic phases in different episodes (Maia et al., 2011; Sibrant et al., 2019). Small (1995) suggested three different model for plume-ridge interaction and discussed the possible volcanism in an off-axis and on-axis scenario. In the present study, presence of intrusive bodies into the crust of the plateau suggests several weak zones which may be associated with faults and rift zones. The modelling result shows intrusive bodies near the ridge axis (Fig. 3b) probably formed by the on-axis volcanism whereas intrusive far from the ridge axis over the plateau suggested to be formed by the off-axis volcanism. Therefore, we believe that the plateau was evolved by off-axis volcanism as well as by on-axis volcanism. Using bathymetry, magnetic and side scan sonar data, Conder et al. (2000) supported the off-axis volcanism over the plateau, whereas other studies (Maia et al., 2011; Sibrant et al., 2019) suggested on-axis volcanism over the plateau. Presence of several normal and reverse polarity magmatic intrusions into the crust of the plateau suggests evolution of the plateau in different magnetic polarity time. The intrusions could have been a major source for basaltic volcanism to the surface of St. Paul and Amsterdam Islands (e.g., Conder et al., 2000; Carvallo et al., 2003). Moreover, the presence of active submarine volcanism reported at the Boomerang seamount (Johnson et al., 2000) indicate that the plume is currently active below the plateau. Another study by Conder et al. (2000) suggested more than one locus of hotspot activity from the plume which might be the reason of magmatic intrusion (in this study) in the ASP plateau.

6.2 Presence of Low Velocity Zone (LVZ) below the ASP plateau?

The observed Low Velocity Zone (LVZ; ~ Vs 4.0 km/s) below Moho (at depth 20-36 km) (Fig. 4c) indicates a possible presence of the magma chamber or partial melt present below the Amsterdam Island. An active magma chamber acts as a sink for magma from a deeper reservoir, which is commonly located in the lower crust or the upper mantle (Becerril et al., 2013). Previous studies also indicate presence of LVZ associated with magma chamber/magma-trap/magma-ponding at the Moho discontinuity beneath Iceland (Derbyshire et al. 2000), Galapagos Island (Villagómez et al., 2007), Azores islands (Zanon, 2015), Valles caldera, New Maxico (Lutter et al. 1995), Teno volcano (Longpre´ et al. 2008) and Mount Fuji (Kinoshita et al. 2015) etc. Magma feeding fissure eruptions ascend through the lithosphere up to the Moho where neutral buoyancy is reached (e.g. Cushman et al. 2004; Schwarz et al. 2004; Nicolosi et al. 2006; Civile et al. 2008; Klu¨gel et al. 2009). However, ascending magmas are not necessarily expected to stagnate at the Moho due to the apparent lack of neutral buoyancy at this interface (Hansteen et al. 1998). But once the neutral buoyancy is reached, the magma chambers near Moho depths may damp the ascent of subsequent magma batches (Clague, 1987).

Morgan (1971) suggested that above the core of the plume, active upwelling plays a major role in melt generation. Buoyant and upwelling mantle lead to decompression melting below the dry solidus (Villagómez et al., 2007). Further, accumulation of melt at the base of the thermal lithosphere creates the observed sharp discontinuity in seismic velocity (Kawakatsu et al., 2009). When the upwelling mantle plume approaches the lithosphere, it begins to flatten and spread at base of the lithosphere forming a low velocity zone at LAB. It is suggested that the magma first interact at the asthenosphere-lithosphere transition in the form of melt, and then further migrates through the lithosphere through dyke propagation (Havlin et al., 2013). We suggest that the magma is possibly stored at the base of the crust and only ascended to the surface using deep active faults. Quilty (2007) reported faults on the Amsterdam and St. Paul islands which might have acted as passage for magma eruption. Our study also reported multiple

intrusive bodies into the crust of ASP plateau. Hence, we propose that the LVZ immediately below Moho at depth of 20-36 km beneath the Amsterdam Island is generated by the combination of melt and excess temperature associated with the plume activity in the form of a magma chamber.

6.3 Horizontal extent of the ASP plume magma supply

The Vertical Gravity Gradient (VGG) map (Fig. 5a) mark the boundary of the AFZ in the north and the SPFZ in the south. Southern part of the SPFZ near the ridge segments (*J2* and *J3*) is not clearly identifiable as these ridge segments are affected by the ASP plume and by presence of thick basaltic crust adjacent to these ridge segments. Royer and Schlich (1988) suggested that the volcanic activity over the plateau was very diffused which altered the normal seafloor spreading magnetic anomalies. Further, Graham et al. (1999) reported that the mantle plume fed the ridge segments *I1*, *I2* and *J1* on the ASP plateau and might be the reason of obscureness. The ridge segment *J2* is less identifiable in its northern half whereas southern half of the ridge is properly reflected in the VGG map, which might indicate that the upper half part is affected by the plume activity, but southern half segment is still unaffected and represents an active ridge segment. Maia et al. (2011) suggested that AFZ acted as a barrier to the volcanism in evolution of the plateau. The VGG results suggest that the ASP plateau is morphologically evolved between the AFZ and SPFZ.

The MBA map (Fig. 5b) clearly shows that the ASP plateau is associated with relatively negative MBA compared to the surrounding oceanic crust. Our gravity-magnetic result reinforces the interpretation that thicker crust (6.6-18 km) and presence of several intrusive bodies associated with the plateau formed by the on-axis as well as off-axis volcanism, causing the negative MBA over the plateau. Below the St. Paul Island, a higher negative MBA is observed probably due to the presence of much lesser dense material caused by the ASP plume activity. Maia et al. (2011) and Janin et al. (2011) suggested the probable location of the ASP hotspot beneath the Amsterdam and St. Paul Islands. Outside the AFZ and SPFZ, the MBA is consistent and positive suggesting presence of a normal oceanic crust unaffected by the plume activity. It is, therefore, clear that these two fracture zones AFZ and SPFZ restricting the magma supply from

the ASP plume beyond the fracture zones and the plume activity is limited beneath the ASP plateau only.

Therefore, based on the interpretation of the VGG and MBA results, we suggest that the ASP plume activity was limited between the AFZ and SPFZ and the plateau was morphologically evolved between the two fracture zones.

6.4 Linkage between the Kerguelen plume and the ASP plateau??

The MBA map (Fig. 5c) represents density variation in the Mantle and If any flow of volcanic material exists between the Kerguelen plume and SEIR that must be reflected in the MBA map as this magmatic flow will display negative MBA due to hotter melt material. The MBA map of the study region shows a linear negative MBA between the ASP plateau and Ninety East Ridge-Broken Ridge along the ASP hot spot track associated with CDP volcanic chain. This linear negative MBA is indicative of less dense material caused by deeper Moho and/or presence of hotter melt materials along the CDP volcanic chain between the ASP plateau and CDP volcanoes. It will be discussed in the section 6.5 that the underplated crust and deeper Moho along the ASP hot spot track is present below the CDP volcanic chain. Previous studies reported underplated crust and deeper Moho below the other hot spot tracks (e.g., Coffin and Eldholm, 1992; Coffin et al., 2002; Fontaine et al., 2015; Kumar et al., 2019; Kumar and Chaubey, 2022). We interpret from the Figure 5c that the MBA below the crust between the Kerguelen and ASP plateau is almost constant and does indicate the absence of hotter melt mantle material and/or showing similar Moho depth. Absence of density variation in the mantle material below this crust suggests that it is not affected by the plume and probably no magma channel is present between these two plateaus. Kerguelen plume is currently active over the Kerguelen plateau since past ~22 Ma (Duncan et al. 2016) and recently volcanic eruption took place at Heard & McDonald Island (Patrick and Smellie, 2013). However, the ASP plume is suggested to be active since ~20 Ma when it formed CDP volcanoes. Eventually from ~10 Ma, it started forming ASP plateau till date. Zhao (2007) has shown a low *P*-wave velocity zone beneath the mantle which is very much closer to the present location of the Kerguelen plateau and might be associated with the Kerguelen plume. It is observed that the low

P-wave velocity zone is quite far from the Amsterdam Island and doesn't show any linkup in the mantle with the ASP plateau. No evidence of channelized flow between the ASP plateau and the Kerguelen plateau in the MBA map concludes that the ASP plateau might not be formed by the Kerguelen plume but was formed by a weaker ASP plume.

6.5 Plume-ridge interaction

We synthesize our results with earlier work to further elucidate the interaction of the ASP plume with the SEIR in time and evolution of the plateau. The ASP volcanic massif forms a morphologically isolated plateau by the ASP plume-SEIR interaction. Previous studies suggested that the ASP plateau is formed during the past 10 My (e.g., Janin et al., 2011; Maia et al., 2011; Janin et al., 2012; Sibuet et al., 2019) and the Chain of Dead Poets (CDP) volcanic is assumed to be the hot spot track of the ASP plume over past ~20 My (e.g., Janin et al., 2011; Maia et al., 2011; Bredow and Steinberger, 2018) and trends age progressively from the southern end of the Ninety East Ridge towards the ASP plateau. Different stages of plume and the SEIR ridge interaction starting from ~20 Ma to present are discussed in detail with the probable on-axis and off-axis volcanism over the plateau. Further, formations of intrusive bodies and magma chamber are also explained in the schematic diagram (Fig. 6).

Since ~20 Ma, the SEIR separated the Antarctic plate and Indo-Australian plate and migrated north-eastward towards the ASP plume, which was situated below the oceanic crust of Australian plate. The ASP plume created a magma chamber through the melts or magma ponds just below the oceanic crust and melted the base of the crust during that time (Fig. 6a). Several magmatic intrusions took place along the weaker zones into the crust in the form of volcanoes leading to the formation of CDP volcanoes (Fig. 6a). During ~15 Ma, as the plate moved further, maximum magma supply at the center of the plume formed magma chambers and series of volcanoes continuously along the ASP hot spot track. Whereas the magma supply decreased to the older magma chambers as the plume moved far from the older chambers causing deficiency in magma supplied to the older magma chambers, cooling the melted material at base of

the crust, and formed underplated crust (Fig. 6b). At the same time, melt extracted through the weak zones or faults in form of intrusions and formed several small and big volcanoes depending on the magma supply. Until ~10 Ma, the ASP plume created several volcanoes of CDP along the hot spot track and underplated the crust below the CDP volcanoes. Richards et al. (2013) suggested high-velocity underplating at the crust-mantle interface beneath several hotspot tracks like the Kerguelen (Coffin and Eldholm, 1992; Coffin et al., 2002), Reunion (Fontaine et al., 2015; Kumar et al., 2019; Kumar and Chaubey, 2022), Cocos ridge (Galapagos hot spot track) (Sallarès et al., 2003) and Louisville hot spot track (Conteras-Reyes et al., 2010) etc. The ASP plateau started forming since ~10 Ma as the SEIR started coming closer to the ASP plume (Fig. 6c) which resulted in the maximum magma supply below the SEIR axis for the formation of the ASP plateau while less magma supplied to the volcanoes located southwest of the CDP volcanic chains simultaneously. Janin et al. (2011) suggested formation of the Boilaeu and La Bruyère seamount (>8 Ma) during this magmatic phase and Janin et al. (2012) suggested formation of the seamounts by interaction of the magma supplied through local depleted mantle and ASP plume magma. We believe that during ~10 to 6 Ma, the Boilaeu and La Bruyère seamount were formed by melt supplied through a magma chamber when the ASP plateau started evolving. The north-eastern part of the ASP plateau was started forming initially during the period ~10 to 6 Ma. Maia et al. (2011) suggested that at slower spreading rate of the SEIR, the connection between the ASP hot spot and SEIR was established at larger distance causing higher magmatic activity during the phase from ~10 to 6 Ma (Sibrant et al., 2019). Maia et al. (2011) suggested an on-axis volcanism for the formation of the plateau. We reported intrusive near the ridge axis (Fig. 3b) in the modeling results which suggest that they were formed probably by the on-axis volcanism. However, it is worth to mention here that several other intrusive (far from the ridge) are also interpreted at the plateau which suggest off-axis volcanism over the plateau. Previous results by Conder et al. (2000) also supported the off-axis volcanism over the ASP plateau. The ASP plume has melted the base of the crust erupting the magma to surface through the faults or weak zones and started forming the ASP plateau (Fig. 6c) probably by off-axis volcanism until the distance between the ASP hot spot and SEIR reduced and a connection between the

plume and ridge established. When the connection between the plume and ridge established or the SEIR reached close to the center of the ASP plume, the magma was supplied from the plume to the ridge and caused an on-axis volcanism over the plateau. We, therefore, believe that the ASP plateau is formed by both the on-axis as well as off-axis volcanism. Further, the first ridge jump took place to southwest of its initial position (Fig. 6d) at ~6.3 Ma (Maia et al., 2011) and paleo ridge-axis acted as a weaker rift zone for the formation of other intrusive bodies. The distance between the SEIR and the ASP plume increased due to the ridge jump and causing weaker connection between them and resulted in less magmatic activity over the plateau as suggested by Maia et al. (2011) and Sibrant et al. (2019) during the phase from 6-3 Ma.

During the phase from 6 to 3 Ma, the distance between the plume and ridge increased due to the ridge jump and the connection between plume and ridge was weakened that further led to the off-axis volcanism over the plateau. Eventually, the plate moved further northeastward, the SEIR started approaching the plume again and age progressively magmatic activity in term of intrusive and lava eruption took place along the plateau (Fig. 6e) by off-axis volcanism. Further, when the SEIR came closer to the plume center, second ridge jump took place at ~3.3 Ma (Maia et al., 2011) and re-located the SEIR at a new axis very close to center of the hot spot (Fig. 6f) marking second phase of higher magmatic activity. The ASP plateau evidenced higher volcanism in this phase as on-axis position of hot spot source gave rise to strong increase in melt supply (Maia et al., 2011) and caused on axis volcanism over the plateau. Further in age progression, SEIR migrated northeastward and crossed the ASP plume positioning below the Antarctica plate towards southwest of the ridge (Fig. 6g). The ridge continued migrating northeastward with increasing distance from the plume up to its present location with a low magmatic activity since ~0.9 Ma (Sibrant et al., 2019) and developed the recently formed Boomerang and St. Pierre volcanoes and Amsterdam & St. Paul islands (Fig. 6h). However, Watkins et al. (1975) suggested that the Amsterdam and St. Paul islands were formed during ~0.4 Ma. Using the bathymetry data, Maia et al. (2011) reported several bathymetry high features over the plateau, which might have formed by the off-axis volcanism by the plume activity. Interpreted intrusions at the Amsterdam and St. Paul Islands and nearby regions suggest an off-axis volcanism since the present

location of the ASP plume is beneath both the islands and is away from any of SEIR ridge segments. Presence of a LVZ at depth of 20-36 km beneath the Amsterdam Island in the present study is the probable source of magma supply to the surface. It may also be noted that the Boomerang seamount is currently an active seamount (Johnson et al., 2000) near the ridge segment I2 and is quite distant from the present location of the plume. However, the Boomerang seamount is getting a magma supply either through the ridge segment fed by the plume or by any active magma chamber. Several submarine volcanoes and seamounts reported over the plateau are associated with bathymetric high features (Maia

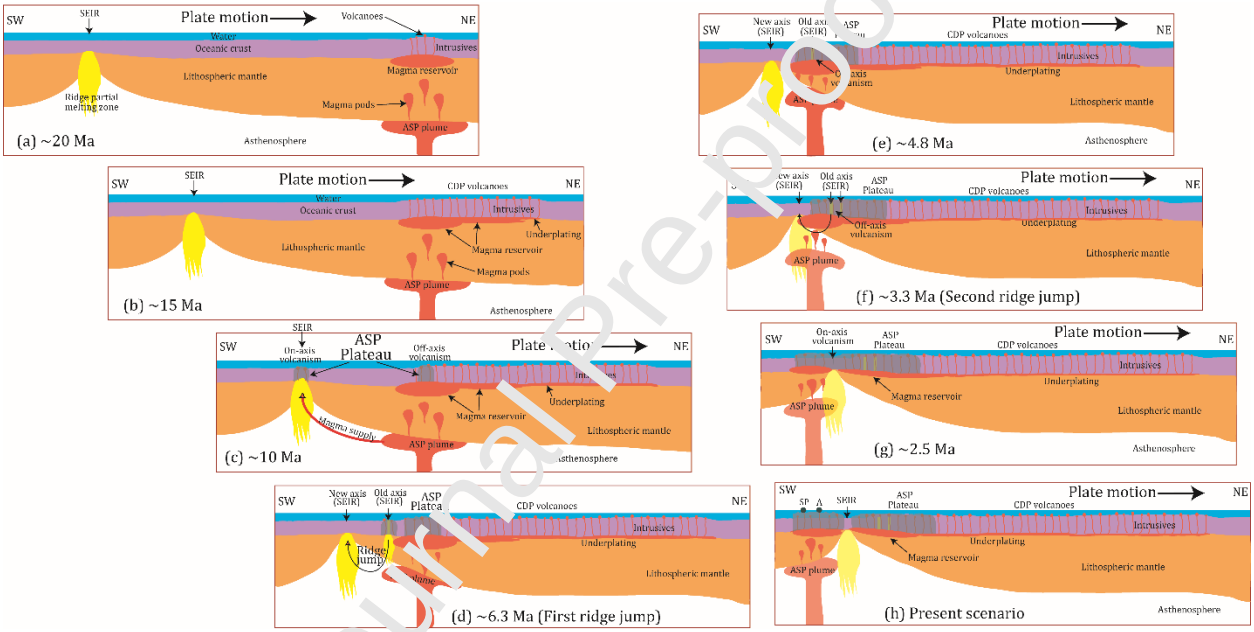

Fig. 6 Schematic diagram depicting interaction of the ASP plume and the SEIR since ~20 Ma in different stages.

et al., 2011; Sibrant et al., 2019). Presence of intrusive in present study and bathymetric highs over the plateau suggest a continuous magma supply to the submarine volcanoes by an active magma chamber. Janin et al. (2011 and 2012) suggested that CDP volcanoes were formed in two generation of magmatic activity; earlier by the ASP plume activity and later by melt migration generated either by plume or depleted mantle or partial melt through the recently formed CDP volcanoes. Presence of low velocity zone below the Amsterdam Island (at depth of 20-36 km, Fig 4c) and negative MBA along the

CDP volcanic chain (Fig. 5b), we believe that magma melt was formed along the ASP hot spot track in the upper mantle. This melt supplied magma to deeper magma chambers which further fed the melts to volcanic magma chambers and erupted onto the surface. Conder et al. (2000) suggested that the new spreading centers acted as channels for transporting melts away from volcanoes and extending the dimensions of the platform by driving the rift propagation. It is worth mentioning that the AFZ and SPFZ played an important role in limiting the horizontal extent of magma chambers, which also suggests a smaller plume head for the ASP mantle plume. Some studies (Sibrant et al., 2019) suggested that the ASP plume is weaker whereas other studies (Courtillot et al., 2003; Janin et al., 2012; Marigneir et al., 2020) suggested the plume to be of deeper in origin.

7. Conclusions

In the present study, we used integrated gravity-magnetic modeling results to determine the crustal architecture of the ASP plateau. Further, we used the results of joint inversion of Ps receiver function and Rayleigh wave group velocity dispersion data to give the upper mantle structure below the Amsterdam Island and the ASP plateau. Analysis and results of geophysical data through integrated approach have provided a new understanding of the crustal architecture and upper mantle structure of the plateau. Major finding of the present study is summarized as follows:

(i) ASP plateau is associated with three crustal layers below the sedimentary strata: basaltic layer (layer 2), gabbroic layer (layer 3) and underplated layer. The results further report presence of several intrusive into the crust of the plateau and suggest both off-axis and on-axis volcanism over the plateau.

(ii) Moho depth ranges from 6.6 to 18 km below the plateau where maximum depth interpreted below the St. Paul Island while minimum Moho depth interpreted outside the plateau. The Moho is interpreted at a depth of ~16 km below the Amsterdam Island.

(iii) A Low Velocity Zone below the crust-mantle boundary (20-36 km depth) beneath the Amsterdam Island is interpreted as signature of a magma chamber. The Lithosphere-Asthenosphere Boundary is interpreted at a depth of 50 km.

(iv) The ASP plume is suggested to be a weaker plume which is bounded between Amsterdam Fracture Zone and St. Paul Fracture Zone. We further suggest that there is no conduit from the Kerguelen plume towards the ASP plateau and the plateau is formed by the ASP plume.

8. Acknowledgement

We are thankful to Ifremer Marine Geosciences, LOUBRIEU Benoît, ROYER Jean-Yves and MAIA Marcia for providing Bathymetry data. We also thank to BEUZART Paul for providing us the ship-borne gravity and magnetic data. This research did not receive any specific grant from funding agencies in the public, commercial, or not-for-profit sectors. This is NGRI contribution number????? and NIO contribution number ????

CRediT authorship contribution statement

Pankaj Kumar: Conceptualization, Methodology, Data curation, Software, Writing- Original draft preparation. **Pabitra Singha:** Conceptualization, Methodology, Data curation, Software, Writing- Review and Editing. **Dibakar Ghosal:** Conceptualization, Supervision, Methodology, Writing- Review and Editing. **Jensen Jacob: Writing**- Review and Editing. **Sandeep Gupta:** Writing- Review and Editing

Data availability statement

For this study, we used the open-source bathymetry, gravity, magnetic and seismological data. The open-source bathymetry data can be found at https://sextant.ifremer.fr/record/342b2892-b0de-4566-bd77-520fb3bf4eaa. The open-source gravity-magnetic data can be downloaded from the link https://campagnes.flotteoceanographique.fr/campagnes/84000111. The seismological datasets can be found from https://ds.iris.edu/wilber3/find_event.

References

Amante, C., and Eakins, B. W. (2009). ETOPO1 arc-minute global relief model: procedures, data sources and analysis.

Ammon, C. J., Randall, G. E., and Zandt, G. (1990). On the nonuniqueness of receiver function inversions. Journal of Geophysical Research: Solid Earth, 95(B10), 15303-15318.

Bathymetry - Saint-Paul and Amsterdam (synthesis, 2020). Ifremer. http://dx.doi.org/10.12770/342b2892-b9de-4566-bd77-520fb3bf4eaa. [Dataset].

Becerril, L., Galindo, I., Gudmundsson, A., & Morales, J. M. (2013). Depth of origin of magma in eruptions. Scientific reports, 3(1), 1-6.

Bhattacharya, S. N. (1983). Higher order accuracy in multiple filter technique. Bulletin of the Seismological Society of America, 73(5), 1395-1406.

Brocher, T. M. (2005). Empirical relations between elastic wavespeeds and density in the Earth's crust. Bulletin of the seismological Society of America, 95(6), 2081-2092.

Bredow, E., and Steinberger, B. (2018). Variable Melt Production Rate of the Kerguelen HotSpot Due To Long-Term Plume-Ridge Interaction. Geophysical Research Letters, 45(1), 126-136.

Ten Brink, U. S., and Brocher, T. M. (1987). Multichannel seismic evidence for a subcrustal intrusive complex under Oahu and a model for Hawaiian volcanism. Journal of Geophysical Research: Solid Earth, 92(B13), 13687-13707.

Beuzart, Paul (1984). HYDROAMSTERDAM cruise, RV Jean Charcot. https://doi.org/10.17600/84000111. [Dataset]
.

Burdick, L.J. and Langston, C.A., 1977. Modeling crustal structure through the use of converted phases in teleseismic body-wave forms. Bulletin of the Seismological Society of America, 67(3), pp.677-691.

Caress, D. W., McNutt, M. K., Detrick, R. S., & Mutter, J. C. (1995). Seismic imaging of hotspot-related crustal underplating beneath the Marquesas Islands. Nature, 373(6515), 600-603.

Carvallo, C., Camps, P., Ruffet, G., Henry, B., and Poidras, T. (2003). Mono Lake or Laschamp geomagnetic event recorded from lava flows in Amsterdam Island (southeastern Indian Ocean). Geophysical Journal International, 154(3), 767-782.

Charvis, P., Laesanpura, A., Gallart, J., Hirn, A., Lépine, J. C., De Voogd, B., Minshull, T. A., Hello, Y., and Pontoise, B. (1999). Spatial distribution of hotspot material added to the lithosphere under La Réunion, from wide-angle seismic data. Journal of Geophysical Research: Solid Earth, 104(B2), 2875-2893.

Christeson, G. L., Goff, J. A., and Reece, R. S. (2019). Synthesis of oceanic crustal structure from two-dimensional seismic profiles. Reviews of Geophysics, 57(2), 504-529.

Civile, D., Lodolo, E., Tortorici, L., Lanzafame, G., and Brancolini, G. (2008). Relationships between magmatism and tectonics in a continental rift: the Pantelleria Island region (Sicily Channel, Italy). Marine Geology, 251(1-2), 32-46.

Clague, D. A. (1987). Hawaiian xenolith populations, magma supply rates, and development of magma chambers. Bulletin of Volcanology, 49(4), 577-587.

Coffin, M. F., and Eldholm, O. (1992). Volcanism and continental break-up: a global compilation of large igneous provinces. Geological Society, London, Special Publications, 68(1), 17-30.

Coffin, M. F., Pringle, M. S., Duncan, R. A., Gladczenko, T. P., Storey, M., Müller, R. D., and Gahagan, L. A. (2002). Kerguelen hotspot magma output since 130 Ma. Journal of Petrology, 43(7), 1121-1137.

Conder, J. A., Scheirer, D. S., and Forsyth, D. W. (2000). Seafloor spreading on the Amsterdam-St. Paul hotspot plateau. Journal of Geophysical Research: Solid Earth. 105(B4), 8263-8277.

Condie K. C., Chapter 2 - The Crust, Editor (s): Kent C. Condie, Earth as an Evolving Planetary System (Third Edition), Academic Press, 2016, Pages 9-41.

Contreras-Reyes, E., Grevemeyer, I., Watts, A. B., Planert, L., Flueh, E. R., and Peirce, C. (2010). Crustal intrusion beneath the Louisville hotspot track. Earth and Planetary Science Letters, 289(3-4), 323-333.

Courtillot, V., Davaille, A., Besse, J., and Stock, J. (2003). Three distinct types of hotspots in the Earth's mantle. Earth and Planetary Science Letters, 205(3-4), 295-308.

Cushman, B., Sinton, J., Ito, G., and Eaby Dixon, J. (2004). Glass compositions, plume-ridge interaction, and hydrous melting along the Galápagos Spreading Center, 90.5° W to 98° W. Geochemistry, Geophysics, Geosystems, 5(8).

Darbyshire, F. A., White, R. S., and Priestley, K. F. (2000). Structure of the crust and uppermost mantle of Iceland from a combined seismic and gravity study. Earth and Planetary Science Letters, 181(3), 409-428.

Di Luccio, F., and Pasyanos, M. E. (2007). Crustal and upper-mantle structure in the Eastern Mediterranean from the analysis of surface wave dispersion curves. Geophysical Journal International, 169(3), 1139-1152.

Doucet, S., Weis, D., Scoates, J. S., Debaille, V., and Giret, A. (2004). Geochemical and Hf-Pb-Sr-Nd isotopic constraints on the origin of the Amsterdam-St. Paul (Indian Ocean) hotspot basalts. Earth and Planetary Science Letters. 218(1-2), 179-195.

Dubinin, E. P., Galushkin, Y. I., Grokholskii, A. L., Kokhan, A. V., and Sushchevskaya, N. M. (2017). Hot and cold zones of the Southeast Indian Ridge and their influence on the peculiarities of its structure and magmatism (Numerical and Physical Modelling). Geotectonics, 51(3), 209-229.

Du, Z. J., and Foulger, G. R. (1999). The crustal structure beneath the northwest fjords, Iceland, from receiver functions and surface waves. Geophysical Journal International, 139(2), 419-432.

Duncan, R. A., Falloon, T. J., Quilty, P. G., and Coffin, M. F. (2016). Widespread Neogene volcanism on Central Kerguelen Plateau, Southern Indian Ocean. Australian Journal of Earth Sciences, 63(4), 379-392.

Ewing, M., and Press, F. (1956). Rayleigh wave dispersion in the period range 10 to 500 seconds. Eos, Transactions American Geophysical Union, 37(2), 213-215.

Fontaine, F. R., Barruol, G., Tkalčić, H., Wölbern, I., Rümpker, G., Bodin, T., and Haugmard, M. (2015). Crustal and uppermost mantle structure variation beneath La Réunion hotspot track. Geophysical Journal International, 203(1), 107-126.

Francis, T. J., and Raitt, R. W. (1967). Seismic refraction measurements in the southern Indian Ocean. Journal of Geophysical Research, 72(12), 3015-3041.

Gallart, J., Driad, L., Charvis, P., Sapin, M., Hirn, A., Diaz, J., de Voogd, B. and Sachpazi, M., 1999. Perturbation to the lithosphere along the hotspot track of La

Réunion from an offshore-onshore seismic transect. Journal of Geophysical Research: Solid Earth, 104(B2), pp.2895-2908.

Gente, P., Dyment, J., Maia, M., and Goslin, J. (2003). Interaction between the Mid-Atlantic Ridge and the Azores hot spot during the last 85 Myr: Emplacement and rifting of the hot spot-derived plateaus. Geochemistry, Geophysics, Geosystems. 4(10).

Georgen, J. E., Lin, J., and Dick, H. J. (2001). Evidence from gravity anomalies for interactions of the Marion and Bouvet hotspots with the Southwest Indian Ridge: Effects of transform offsets. Earth and Planetary Science Letters, 187(3-4), 283-300.

Graham, D. W., Johnson, K. T. M., Priebe, L. D., and Lupton, J. E. (1999). Hotspot-ridge interaction along the Southeast Indian Ridge near Amsterdam and St. Paul islands: helium isotope evidence. Earth and Planetary Science Letters, 167(3-4), 297-310.

Green, R. G., Priestley, K. F., and White, R. S. (2017). Ambient noise tomography reveals upper crustal structure of Icelandic rifts. Earth and Planetary Science Letters, 466, 20-31.

Grevemeyer, I., Weigel, W., Schüssler, S. and Avedik, F. (2001). Crustal and upper mantle seismic structure and lithospheric flexure along the Society Island hotspot chain. Geophysical Journal International, 147(1), 123-140.

Gupta, Sandeep, Mishra, S. and Rai, S.S. (2010). Magmatic underplating of crust beneath the Laccadive Island, NW Indian Ocean. Geophysical Journal International, 183, 536-542.

Gupta S., Borah K., and Saha G., 2016, Continental like crust beneath the Andaman Island through joint inversion of receiver function and surface wave from ambient seismic noise, Tectonophysics, 687, 129-138.

Hansteen, T. H., Klügel, A., and Schmincke, H. U. (1998). Multi-stage magma ascent beneath the Canary Islands: evidence from fluid inclusions. Contributions to Mineralogy and Petrology, 132(1), 48-64.

Havlin, C., Parmentier, E. M., and Hirth, G. (2013). Dike propagation driven by melt accumulation at the lithosphere-asthenosphere boundary. Earth and Planetary Science Letters, 376, 20-28.

Herrmann, R. B. (1973). Some aspects of band-pass filtering of surface waves. Bulletin of the Seismological Society of America, 63(2), 663-671.

Herrmann, R. B. (2013). Computer programs in seismology: An evolving tool for instruction and research. Seismological Research Letters, 84(6), 1081-1088.

Janin, M., Hémond, C., Guillou, H., Maia, M., Johnson, K. T. M., Bollinger, Liorzou, C. and Mudholkar, A. (2011). Hot spot activity and tectonic settings near Amsterdam-St. Paul plateau (Indian Ocean). Journal of Geophysical Research: Solid Earth, 116(B5).

Janin, M., Hémond, C., Maia, M., Nonnotte, P., Ponzevera, E., and Johnson, K. T. M. (2012). The Amsterdam-St. Paul Plateau: A complex hot spot/DUPAL flavored MORB interaction. Geochemistry, Geophysics, Geosystems. 13(9).

Jenkins, J., Maclennan, J., Green, R. G., Cottaar, S., Deuss, A. F., and White, R. S. (2018). Crustal formation on a spreading ridge above a mantle plume: receiver function imaging of the Icelandic crust. Journal of Geophysical Research: Solid Earth, 123(6), 5190-5208.

Johnson, G. L., Southall, J. R., Young, P. W., and Vogt, P. R. (1972). Origin and structure of the Iceland Plateau and Kolbeinsey Ridge. Journal of Geophysical Research. 77(29), 5688-5696.

Johnson, K. T. M., Graham, D. W., Rubin, K. H., Nicolaysen, K., Scheirer, D. S., Forsyth, D. W., Baker, E. T., and Douglas-Priebe, L. M. (2000). Boomerang seamount: the active expression of the Amsterdam-St. Paul hotspot, Southeast Indian Ridge. Earth and Planetary Science Letters, 183(1-2), 245-259.

Julia, J., Ammon, C. J., Herrmann, R. B., and Correig, A. M. (2000). Joint inversion of receiver function and surface wave dispersion observations. Geophysical Journal International, 143(1), 99-112.

Kawakatsu, H., Kumar, P., Takei, Y., Shinohara, M., Kanazawa, T., Araki, E., and Suyehiro, K. (2009). Seismic evidence for sharp lithosphere-asthenosphere boundaries of oceanic plates. science, 324(5926), 499-502.

Kinoshita, S. M., Igarashi, T., Aoki, Y., and Takeo, M. (2015). Imaging crust and upper mantle beneath Mount Fuji, Japan, by receiver functions. Journal of Geophysical Research: Solid Earth, 120(5), 3240-3254.

Klügel, A., Hansteen, T. H., and Galipp, K. (2005). Magma storage and underplating beneath Cumbre Vieja volcano, la Palma (Canary Islands). Earth and Planetary Science Letters, 236(1-2), 211-226.

Kumar, P., and Chaubey, A. K. (2022). Réunion plume associated flood basalt volcanism on the northwestern continental margin of India and related tectonics. Journal of Asian Earth Sciences, 105352.

Kumar, P., Kind, R., Hanka, W., Wylegalla, K. R. C. H., Reigber, C., Yuan, X., Woelbern, I., Schwintzer, P., Fleming, K., Dahl-Jensen, T., Larsen, T.B., Schweitzer, J., Priestley, K., Gudmundsson, O., and Wolf, D. (2005). The lithosphere-asthenosphere

boundary in the North-West Atlantic region. Earth and Planetary Science Letters, 236(1-2), 249-257.

Kumar, P., Mishra, A., Pitchika, V. K., Kumar, S., Dubey, K. M., Singh, D., and Chaubey, A. K. (2019). Integrated geophysical appraisal of crustal structure and tectonic evolution of the Angria Bank, western continental margin of India. Marine Geophysical Research, 40(3), 433-449.

Kumar, P., Yuan, X., Kumar, M. R., Kind, R., Li, X., and Chadha, R. K. (2007). The rapid drift of the Indian tectonic plate. Nature, 449(7164), 894-897.

Ligorría, J. P., and Ammon, C. J. (1999). Iterative deconvolution and receiver-function estimation. Bulletin of the seismological Society of America, 89(5), 1395-1400.

Longpré, M. A., Troll, V. R., and Hansteen, T. H. (2008). Upper mantle magma storage and transport under a Canarian shield-volcano, Teno, Tenerife (Spain). Journal of Geophysical Research: Solid Earth, 113(B8).

Ludden, J. N., Thompson, G., Bryan, W. B., and Frey, F. A. (1980). The origin of lavas from the Ninetyeast Ridge, Eastern Indian Ocean: an evaluation of fractional crystallization models. Journal of Geophysical Research: Solid Earth, 85(B8), 4405-4420.

Lutter, W.J., Roberts, P.M., Thurber, C.H., Steck, L., Fehler, M.C., Stafford, D.G., Baldridge, W.S. and Zeichert, T.A. (1995). Teleseismic P-wave image of crust and upper mantle structure beneath the Valles Caldera, New Mexico: Initial Results from the 1993 JTEX Passive Array. Geophysical research letters, 22(4), 505-508.

Luyendyk, B. P., and Rennick, W. (1977). Tectonic history of aseismic ridges in the eastern Indian Ocean. Geological Society of America Bulletin, 88(9), 1347-1356.

Maia, M., Pessanha, I., Courrèges, E., Patriat, M., Gente, P., Hémond, C., Janin, M., Johnson, K., Roest, W., Royer, J.Y. and Vatteville, J. (2011). Building of the Amsterdam-Saint Paul plateau: A 10 Myr history of a ridge-hot spot interaction and variations in the strength of the hot spot source. Journal of Geophysical Research: Solid Earth. 116(B9).

Marignier, A., Ferreira, A. M., and Kitching, T. (2020). The probability of mantle plumes in global tomographic models. Geochemistry, Geophysics, Geosystems, 21(9), e2020GC009276.

Morgan, W. J. (1971). Convection plumes in the lower mantle. Nature, 230(5288), 42-43.

Morgan, W. J. (1978). Rodriguez, Darwin, Amsterdam,..., a second type of hotspot island. Journal of Geophysical Research: Solid Earth. 83(B11), 5355-5360.

Menke, W. (1984). Geophysical data analysis: Discrete inverse theory: Academic Presss.

Mutter, J. C., and Cande, S. C. (1983). The early opening between Broken Ridge and Kerguelen Plateau. Earth and Planetary Science Letters. 65(2), 369-376.

Nicolaysen, K. P., Frey, F. A., Mahoney, J. J., Johnson, K. T. M., and Graham, D. W. (2007). Influence of the Amsterdam/St. Paul hot spot along the Southeast Indian Ridge between 77 and 88 E: Correlations of Sr, Nd, Pb, and He isotopic variations with ridge segmentation. Geochemistry, Geophysics, Geosystems. 8(9).

Owens, T.J., Zandt, G. and Taylor, S.R., 1984. Seismic evidence for an ancient rift beneath the Cumberland Plateau, Tennessee: A detailed analysis of broadband teleseismic P waveforms. Journal of Geophysical Research: Solid Earth, 89(B9), pp.7783-7795.

Özalaybey, S., Savage, M. K., Sheehan, A. F., Louie, J. N., and Brune, J. N. (1997). Shear-wave velocity structure in the northern Basin and Range province from the combined analysis of receiver functions and surface waves. Bulletin of the Seismological Society of America, 87(1), 183-199.

Parker, R. L. (1972). The rapid calculation of potential anomalies. Geophysical Journal International, 31(4), 447-455.

Patrick, M. R., and Smellie, J. L. (2013). Synthesis A spaceborne inventory of volcanic activity in Antarctica and southern oceans, 2000-10. Antarctic Science, 25(4), 475-500.

Quilty, P. G. (2007). Origin and evolution of the sub-Antarctic islands: the foundation. In Papers and Proceedings of the Royal Society of Tasmania, 141(1), 35-58).

Richards, M., Contreras-Reyes, E., Lithgow-Bertelloni, C., Ghiorso, M., and Stixrude, L. (2013). Petrological interpretation of deep crustal intrusive bodies beneath oceanic hotspot provinces. Geochemistry, Geophysics, Geosystems, 14(3), 604-619.

Royer, J. Y., and Schlich, R. (1988). Southeast Indian Ridge between the Rodriguez triple junction and the Amsterdam and Saint-Paul islands: Detailed kinematics for the past 20 my. Journal of Geophysical Research: Solid Earth, 93(B11), 13524-13550.

Rychert, C. A., Harmon, N., and Armitage, J. J. (2018). Seismic imaging of thickened lithosphere resulting from plume pulsing beneath Iceland. Geochemistry, Geophysics, Geosystems, 19(6), 1789-1799.

Rychert, C. A., Harmon, N., and Ebinger, C. (2014). Receiver function imaging of lithospheric structure and the onset of melting beneath the Galápagos Archipelago. Earth and Planetary Science Letters, 388, 156-165.

Sallarès, V., Charvis, P., Flueh, E. R., and Bialas, J. (2003). Seismic structure of Cocos and Malpelo Volcanic Ridges and implications for hot spot-ridge interaction. Journal of Geophysical Research: Solid Earth, 108(B12).

Sallarès, V., Charvis, P., Flueh, E. R., Bialas, J., v SALIERI Scientific Party. (2005). Seismic structure of the Carnegie ridge and the nature of the Galapagos hotspot. Geophysical Journal International, 161(3), 763-788.

Sandwell, D. T., Müller, R. D., Smith, W. H., Garcia, E., and Francis, R. (2014). New global marine gravity model from CryoSat-2 and Jason-1 reveals buried tectonic structure. Science, 346(6205), 65-67.

Scheirer, D. S., Baker, E. T., and Johnson, K. T. (1998). Detection of hydrothermal plumes along the Southeast Indian Ridge near the Amsterdam-St. Paul Plateau. Geophysical Research Letters, 25(1), 97-100.

Scheirer, D. S., Forsyth, D. W., Conder, J. A., Eberle, M. A., Hung, S. H., Johnson, K. T., and Graham, D. W. (2000). Anomalous seafloor spreading of the Southeast Indian Ridge near the Amsterdam-St. Paul plateau. Journal of Geophysical Research: Solid Earth, 105(B4), 8243-8262.

Schilling, J. G., Thompson, G., Kingsley, R., and Humphris, S. (1985). Hotspot-migrating ridge interaction in the South Atlantic. Nature. 313(5999), 187-191.

Schlindwein, V. (2006). On the use of teleseismic receiver functions for studying the crustal structure of Iceland. Geophysical Journal International, 164(3), 551-568.

Sibrant, A. L. R., Maia, M., Mittelstaedt, E., and Graham, D. W. (2019). Variable crustal production originating from mantle source heterogeneity beneath the South East Indian Ridge and Amsterdam-St. Paul Plateau. Geochemistry, Geophysics, Geosystems. 20(11), 4635-4653.

Small, C. (1995). Observation of ridge-hotspot interactions in the Southern Ocean. Journal of Geophysical Research: Solid Earth, 100(B9), 17931-17946.
Spieker, K., Rondenay, S., Ramalho, R., Thomas, C., & Helffrich, G. (2018). Constraints on the structure of the crust and lithosphere beneath the Azores Islands from teleseismic receiver functions. Geophysical Journal International, 213(2), 824-835.

Straume, E.O., Gaina, C., Medvedev, S., Hochmuth, K., Gohl, K., Whittaker, J. M., et al. (2019). GlobSed: Updated total sediment thickness in the world's oceans. Geochemistry, Geophysics, Geosystems, 20.

Tkalčić, H., Pasyanos, M. E., Rodgers, A. J., Gök, R., Walter, W. R., and Al-Amri, A. (2006). A multistep approach for joint modeling of surface wave dispersion and

teleseismic receiver functions: Implications for lithospheric structure of the Arabian Peninsula. Journal of Geophysical Research: Solid Earth, 111(B11).

Talwani, M., Worzel, J. L., and Landisman, M. (1959). Rapid gravity computations for two-dimensional bodies with application to the Mendocino submarine fracture zone. Journal of geophysical research, 64(1), 49-59.

Talwani, M., Heirtzler, J.R., 1964. Computation of Magnetic anomalies caused by twodimensional structures of arbitrary shape. In: Parks, G.A. (Ed.), Computers in the Mineral Industries. Stanford University, 464-480.

Tikku, A. A., and Cande, S. C. (2000). On the fit of Broken Ridge and Kerguelen plateau. Earth and Planetary Science Letters. 180(1-2), 117-132.

Ten Brink, U. S., and Brocher, T. M. (1987). Multichannel seismic evidence for a subcrustal intrusive complex under Oahu and a model for Hawaiian volcanism. Journal of Geophysical Research: Solid Earth, 92(B13), 13687-13707.

Villagómez, D. R., Toomey, D. R., Hooft, E. E., and Solomon, S. C. (2007). Upper mantle structure beneath the Galápagos Arcnipelago from surface wave tomography. Journal of Geophysical Research: Solid Earth, 112(B7).

Watkins, N. D., McDougall, I., and Nougier, J. (1975). Paleomagnetism and potassium-argon age of St. Paul Island, southeastern Indian Ocean: Contrasts in geomagnetic secular variation during the Brunhes Epoch. Earth and Planetary Science Letters. 24(3), 377-384.

Watts, A. B., Ten Brink, U. S., Buhl, P., and Brocher, T. M. (1985). A multichannel seismic study of lithospheric flexure across the Hawaiian-Emperor seamount chain. Nature, 315(6015). 105-111.

White, R. S., McKenzie, D., and O'Nions, R. K. (1992). Oceanic crustal thickness from seismic measurements and rare earth element inversions. Journal of Geophysical Research: Solid Earth, 97(B13), 19683-19715.

Won, I. J., and Bevis, M. (1987). Computing the gravitational and magnetic anomalies due to a polygon: Algorithms and Fortran subroutines. Geophysics, 52(2), 232-238.

Wilson, D. S., and Hey, R. N. (1995). History of rift propagation and magnetization intensity for the Cocos-Nazca sspreading Center. Journal of Geophysical Research: Solid Earth. 100(B6), 10041-10056.

Zanon, V. (2015). Conditions for mafic magma storage beneath fissure zones at oceanic islands. The case of São Miguel island (Azores archipelago). Geological Society, London, Special Publications, 422(1), 85-104.

Zhao, D. (2007). Seismic images under 60 hotspots: search for mantle plumes. Gondwana Research, 12(4), 335-355.

Declaration of interests

☒The authors declare that they have no known competing financial interests or personal relationships that could have appeared to influence the work reported in this paper.

☐The authors declare the following financial interests/personal relationships which may be considered as potential competing interests:

Highlights:

- The Amsterdam-St. Paul (ASP) plateau is associated with basaltic, gabbroic and underplated layer below sedimentary strata.
- A low velocity zones below the Moho (20-36 km depth) indicate magma chamber beneath the Amsterdam Island.
- The Lithosphere-Asthenosphere boundary is present at ~50 km depth.
- The ASP plateau might not be formed by the Kerguelen plume.